J. Fluid Mech. (2001), *vol.* 447, *pp.* 85–109. © 2001 Cambridge University Press
DOI: 10.1017/S0022112001005778 Printed in the United Kingdom

One-dimensional turbulence: vector formulation and application to free shear flows

By ALAN R. KERSTEIN[1]†, W. T. ASHURST[1], SCOTT WUNSCH[1] AND VEBJORN NILSEN[2]

[1]Combustion Research Facility, Sandia National Laboratories, Livermore, CA 94551-0969, USA
[2]Torrex Equipment Corporation, Livermore, CA 94550, USA

(Received 14 February 2001 and in revised form 15 May 2001)

One-dimensional turbulence is a stochastic simulation method representing the time evolution of the velocity profile along a notional line of sight through a turbulent flow. In this paper, the velocity is treated as a three-component vector, in contrast to previous formulations involving a single velocity component. This generalization allows the incorporation of pressure-scrambling effects and provides a framework for further extensions of the model. Computed results based on two alternative physical pictures of pressure scrambling are compared to direct numerical simulations of two time-developing planar free shear flows: a mixing layer and a wake. Scrambling based on equipartition of turbulent kinetic energy on an eddy-by-eddy basis yields less accurate results than a scheme that maximizes the intercomponent energy transfer during each eddy, subject to invariance constraints. The latter formulation captures many features of free shear flow structure, energetics, and fluctuation properties, including the spatial variation of the probability density function of a passive advected scalar. These results demonstrate the efficacy of the proposed representation of vector velocity evolution on a one-dimensional domain.

1. Introduction

The correlated fluctuations of velocity and pressure in incompressible turbulence are among the most challenging aspects of turbulence from a modelling perspective, owing to the non-local nature of pressure-field evolution. Nevertheless, empirical approaches based on concepts such as return to isotropy provide useful representations of pressure–velocity correlations in closure-based models (Pope 2000). These models empirically characterize the rate of return to isotropy on an ensemble averaged basis.

In contrast, the modelling approach adopted here involves an unsteady simulation of flow evolution that is resolved in space and time. The model incorporates an explicit representation of the kinematics and dynamics of velocity-field evolution during individual eddy turnovers.

This approach provides a more direct connection between model assumptions and the phenomenology of pressure-fluctuation effects than is possible for models based on time or ensemble averaging. Reynolds-stress models and their probability-density-function (PDF) counterparts require strongly coupled flow interactions to be represented as multiple subprocesses whose physical significance is unclear in some instances. Models of this type that address details of flow structure are generally

† Author to whom correspondence should be addressed: e-mail kerstein@ca.sandia.gov

https://doi.org/10.1017/S0022112001005778 Published online by Cambridge University Press

limited to a particular class of flows, as illustrated by recent applications to free shear flows (Kim & Chung 1995; Van Slooten, Jayesh & Pope 1998) and near-wall flows (Dreeben & Pope 1998), respectively.

The present focus is simulation of free shear flows. In the flows considered here, the dominant pressure–velocity interactions are inviscid at high Reynolds number (*Re*), simplifying the interpretation of results. Nevertheless, viscous effects are fully represented within the model, so the formulation introduced here is directly applicable to boundary layers and other flows (Kerstein *et al.* 2001).

The model introduced here is a generalization of 'one-dimensional turbulence' (ODT). ODT is an unsteady simulation of a velocity profile on a one-dimensional domain representing a notional line of sight through a turbulent flow. Because vortical overturns cannot occur in continuum flow on a one-dimensional domain, a stochastic process, involving instantaneous mappings that represent individual overturns, is introduced. Conventional continuum representations of molecular processes such as viscous transport are implemented on the one-dimensional domain.

The model was originally (Kerstein 1999*a*) formulated to evolve the profile of a single velocity component because it lacked a representation of interaction among velocity components. Recently (Wunsch & Kerstein 2001), a method was introduced for modifying component energy while obeying all conservation and consistency requirements. The method was applied to a buoyant stratified flow for which conversion between kinetic and potential energy was the key concern, so implications for modelling energy transfer among velocity components were not addressed. Here, the model is generalized by introducing a vector velocity field whose three components exchange energy in a manner that emulates pressure–velocity interactions.

The description of the new formulation (§ 2) is followed by its application to time-developing free shear flows for which detailed flow statistics, and some passive scalar statistics, are available from direct numerical simulations (DNS) by Rogers & Moser (1994) and Moser, Rogers & Ewing (1998). These are useful initial comparison cases because the self-similar regimes of these flows exhibit intricacies of flow energetics that provide stringent tests of a turbulence model, yet are insensitive to viscous-scale processes. Thus, the focus of model comparisons to DNS is the model representation of inviscid energy transfer, which is the novel feature of the present formulation. Application of the vector velocity formulation to turbulent boundary layers, in which viscous processes play a key role, is reported elsewhere (Kerstein *et al.* 2001).

2. Stochastic simulation method

2.1. *Overview*

The advantages of a turbulence model formulated as a one-dimensional unsteady stochastic simulation are twofold. First, a one-dimensional formulation enables affordable simulation of high-*Re* turbulence over the full range of dynamically relevant length scales, allowing physically sound representation of interactions between turbulent advection and microphysical processes such as viscous dissipation. Second, this approach captures diverse flow behaviours within a concise modelling framework based on broadly applicable empirical principles, thereby demonstrating a degree of commonality among turbulent flow phenomena that might not otherwise be readily apparent.

Since the present model formulation is a substantial generalization of earlier formulations, a detailed description is provided here. This version of ODT describes

https://doi.org/10.1017/S0022112001005778 Published online by Cambridge University Press

the evolution of a three-component vector velocity field $v_i(y,t)$ defined on a one-dimensional domain (parameterized by the spatial coordinate y, corresponding to the direction $i = 2$). Additional scalar fields $\theta(y,t)$ may also be defined in the model.

The fields defined on the one-dimensional domain evolve by two mechanisms: molecular evolution and a stochastic process representing advection. The stochastic process consists of a sequence of events, each of which involves an instantaneous transformation of the velocity and scalar fields. During the time interval between each event and its successor, molecular evolution occurs, governed by the equations

$$(\partial_t - \nu\partial_y^2)v_i(y,t) = 0, \tag{1}$$

$$(\partial_t - \kappa\partial_y^2)\theta(y,t) = 0, \tag{2}$$

where ν is the kinematic viscosity and κ is the scalar diffusivity (from which the Schmidt number, $Sc = \nu/\kappa$, is formed).

The events representing advection may be interpreted as the model analogue of individual turbulent eddies. This interpretation is not essential to the analysis; it merely provides an intuitive basis for presenting the model. In what follows, these events are termed 'eddy events' or simply eddies. This terminology reflects the fact that each event is characterized by three properties, namely a length scale, a time scale, and a measure of kinetic energy, and a key physical input to the model is a postulated relationship among these quantities that is analogous to the usual dimensional relationship applied to individual turbulent eddies.

The advection submodel is specified by defining the mathematical operations performed during an eddy event and by formulating the rules that govern the random selection of events. Roughly speaking, the eddy definition is the model representation of flow kinematics (i.e. fluid advection and flow-field response to forcings), while rules governing the stochastic selection of events reflect the dynamics that drive the eddy motions.

Because advection is implemented as an event sequence rather than a continuous process, the velocity field does not directly prescribe the fluid motions. Motions and velocities are nevertheless closely linked through the dynamics embodied in the event selection rules (§ 2.3).

In the current formulation, an eddy event consists of two mathematical operations. One is a measure-preserving map representing the fluid motions associated with a notional turbulent eddy. The other is a modification of the velocity profiles in order to implement energy transfers prescribed by the dynamical rules. These operations are represented symbolically as

$$v_i(y) \to v_i(f(y)) + c_i K(y), \quad \theta(y) \to \theta(f(y)). \tag{3}$$

According to this prescription, fluid at location $f(y)$ is moved to location y by the mapping operation, thus defining the map in terms of its inverse $f(y)$, which is convenient for present purposes. This mapping, which is the model analogue of the advection operator $\boldsymbol{v}\cdot\nabla$ of the Navier–Stokes equations, is applied to all fluid properties. The additive term $c_i K(y)$, affecting only the velocity components, represents velocity changes due to pressure gradients or body forces. This additional term was introduced by Wunsch & Kerstein (2001) in order to capture aspects of buoyant stratified flow energetics in a formulation involving one velocity component. Here it is used in a vector velocity formulation to capture pressure-induced energy redistribution among velocity components.

The functional form chosen for $f(y)$ is the simplest of a class of mappings that

https://doi.org/10.1017/S0022112001005778 Published online by Cambridge University Press

satisfy the physical requirements of measure preservation (the non-local analogue of vanishing velocity divergence), continuity (no introduction of discontinuities by the mapping operation), and scale locality (at most order-unity changes in property gradients). The first two requirements are fundamental properties. The requirement of scale locality is based on the well-established empirical principle that length-scale reduction in a turbulent cascade occurs by a sequence of small steps (corresponding to notional turbulent eddies), causing downscale energy transfer to be effectively local in wavenumber. Kerstein (1999*a*) discusses possible definitions of $f(y)$ with reference to these and other desired attributes, and adopts the 'triplet map,'

$$f(y) \equiv y_0 + \begin{cases} 3(y-y_0) & \text{if } y_0 \leqslant y \leqslant y_0 + \frac{1}{3}l \\ 2l - 3(y-y_0) & \text{if } y_0 + \frac{1}{3}l \leqslant y \leqslant y_0 + \frac{2}{3}l \\ 3(y-y_0) - 2l & \text{if } y_0 + \frac{2}{3}l \leqslant y \leqslant y_0 + l \\ y - y_0 & \text{otherwise,} \end{cases} \tag{4}$$

that was employed in an earlier (Kerstein 1991) one-dimensional mixing model. This mapping takes a line segment $[y_0, y_0+l]$, shrinks it to a third of its original length, and then places three copies on the original domain. The middle copy is reversed, which maintains the continuity of advected fields and introduces the rotational folding effect of turbulent eddy motion. Property fields outside the size-l segment are unaffected. The parameters y_0 and l determining the segment location and size are specified for a given event by random sampling, governed by rules explained in § 2.3.

In (3), K is a kernel function that is conveniently defined as $K(y) = y - f(y)$. It is non-zero only within the eddy interval, and it integrates to zero so that energy redistribution does not change the total (y-integrated) momentum of individual velocity components (here assuming constant density). The amplitudes c_i in (3) are determined for each eddy individually according to a pressure-scrambling model that is described next.

2.2. *Pressure-scrambling model*

A mechanism for pressure scrambling is introduced that changes the kinetic energy of individual velocity components, defined by

$$E_i \equiv \tfrac{1}{2}\rho_0 \int v_i^2(y)\,\mathrm{d}y, \tag{5}$$

while keeping the total kinetic energy $E \equiv \sum_i E_i$ constant. (In this section, the argument t of v_i and functions of v_i is suppressed. For convenience, the density ρ_0, assumed constant, is defined as mass per unit length. Applications considered here are unaffected by the definition or value of the density.) This is accomplished by adding the function $K(y)$ to each component with a prescribed amplitude c_i, as indicated in (3). Determination of these amplitudes requires additional modeling.

To formulate this part of the model, we consider the change in the kinetic energy of component i due to the implementation of an eddy event. According to (3), the energy change is

$$\Delta E_i = \tfrac{1}{2}\rho_0 \int [(v_i(f(y)) + c_i K(y))^2 - v_i(y)^2]\mathrm{d}y = \rho_0 l^2 c_i (v_{i,K} + \tfrac{2}{27} l c_i), \tag{6}$$

where we have used the identity $\int K^2(y)\,\mathrm{d}y = \frac{4}{27}l^3$ and the definition

$$v_{i,K} \equiv \frac{1}{l^2}\int v_i(f(y))K(y)\,\mathrm{d}y = \frac{4}{9l^2}\int_{y_0}^{y_0+l} v_i(y)[l - 2(y-y_0)]\,\mathrm{d}y. \tag{7}$$

https://doi.org/10.1017/S0022112001005778 Published online by Cambridge University Press

The rightmost expression in (7) follows from the definitions of $f(y)$ and $K(y)$. The requirement $\sum_i \Delta E_i = 0$ implies only one constraint on the three amplitudes c_i.

Motivated by the phenomenological interpretation of pressure scrambling as a tendency to restore isotropy, the amplitudes are further constrained by requiring invariance under exchange of indices. With these constraints, the kinetic energy changes imposed on the velocity components must be of the form

$$\Delta E_i = \alpha \sum_j T_{ij} Q_j, \tag{8}$$

where Q_j ($j = 1$, 2, or 3) is a quantity with units of energy that depends on $v_j(y)$ and scalars, α is a free parameter, and the transfer matrix $\boldsymbol{T}$ is defined by

$$\boldsymbol{T} \equiv \frac{1}{2} \begin{pmatrix} -2 & 1 & 1 \\ 1 & -2 & 1 \\ 1 & 1 & -2 \end{pmatrix}. \tag{9}$$

This matrix is constructed to obey energy conservation ($\sum_i \Delta E_i = 0$) and to be invariant under permutation of indices. These requirements uniquely define $\boldsymbol{T}$ except for an arbitrary multiplicative constant, which is absorbed in the parameter α. Using (6), the amplitudes c_i are determined by the choice of the quantities Q_i and the value of α.

Specification of Q_i is motivated by the following observation. While addition of $c_i K(y)$ to v_i makes it possible to add an arbitrarily large quantity of energy, the amount that can be removed is bounded. The bound is determined by maximizing $-\Delta E_i$ with respect to c_i in (6). It is advantageous to set Q_i equal to this bound because α is then conveniently interpreted as the energy extracted from each velocity component, expressed as fraction of the maximum possible energy extracted, for redistribution to the other components. The physically realizable range of α is then [0,1], regardless of the instantaneous structure of the v_i fields. For this choice of Q_i, particular values of α have natural physical interpretations, as noted in § 3.1. On this basis, we obtain

$$Q_i \equiv \tfrac{27}{8} \rho_0 l v_{i,K}^2. \tag{10}$$

Wunsch & Kerstein (2001) note that Q_i defined in this manner is also a useful measure of eddy kinetic energy for other purposes; in § 2.3 it is used in the formulation of eddy selection rules. We will refer to Q_i as defined in (10) as the 'available kinetic energy' of velocity component i in the interval $[y_0, y_0 + l]$.

Because the available kinetic energy as defined here is based on a model construct, it does not have a fundamental basis in the same sense as the thermodynamic concept of available work (Callen 1960) or the available potential energy concept applied to density-stratified flow (Lorenz 1955). However, the procedure formulated here for implementing energy changes is broadly consistent with the empirical principle of scale locality. The function $K(y)$ introduced in (3) concisely embodies this principle by assuring that (i) the scale of velocity fluctuations induced by energy transfers is comparable to the eddy size, and (ii) fluctuations that determine the energy available for transfer, based on (6), are of comparable size. Analogous considerations apply to the role of $K(y)$ in the eddy selection process, § 2.3.

With Q_i given by (10), the exchange amplitudes c_i are obtained by solving (6)–(9)

https://doi.org/10.1017/S0022112001005778 Published online by Cambridge University Press

to obtain

$$c_i = \frac{27}{4l}\left(-v_{i,K} + \mathrm{sgn}(v_{i,K})\sqrt{v_{i,K}^2 + \alpha\sum_j T_{ij}v_{j,K}^2}\right). \tag{11}$$

The solution is guaranteed to be real provided that $0 \leqslant \alpha \leqslant 1$, reflecting the physical constraints on the range of α.

In (11), the sign ambiguity in the solution to the quadratic equation for c_i is resolved by requiring that $c_i \to 0$ as $\alpha \to 0$. Velocity components that are initially zero everywhere are seeded with small initial random perturbations to prevent sign ambiguities in these components. The perturbations are symmetric about zero, assuring that these components have zero mean unless a boundary condition or body forcing breaks the symmetry. In general, the model formulation as outlined is consistent with the ensemble-average symmetry and invariance properties of the specified initial and boundary conditions and forcings, though instantaneous flow states do not satisfy these properties due to random fluctuations.

2.3. *Eddy selection*

The final ingredient required in the model is the determination of the time sequence of eddy events, individually parameterized by position y_0 and size l, that are implemented. In ODT, eddy events are implemented instantaneously, but should occur with frequencies comparable to the turnover frequencies of corresponding turbulent eddies. Events are therefore sampled from an event rate distribution that reflects the physics governing eddy turnovers. A key feature of this distribution is that it based on the instantaneous state of the flow, and thus evolves in time as the flow evolves.

At each instant in time, the event rate distribution is defined by first associating a time scale $\tau(y_0, l)$ with every possible eddy event. This time scale is analogous to the eddy turnover time as usually defined, but with a crucial difference. It is based on the instantaneous velocity profiles $v_i(y, t)$ rather than some presumed 'characteristic' velocity fluctuation amplitude across a given size-l eddy, so no *a priori* scaling *ansatz* is required. Time scales of individual eddy events can and do deviate significantly from the values that would be inferred from conventional estimates of the turnover times of 'typical' size-l eddies. The simulated flow evolution reflecting these eddy events and their interactions (through the 'imprint' of individual events on the velocity profiles and the consequent memory of past events) is found to reproduce the salient features and scalings of turbulent eddy cascades (Kerstein 1999*a*; Wunsch & Kerstein 2001), which are thus outcomes of the model rather than inputs to the model. This attribute of the model is illustrated in the present context by results presented in § 3.1.

For a quantititive definition of τ, a measure of the turbulent kinetic energy associated with each possible mapping interval is employed. The most general dimensionally consistent form for the time scales $\tau(y_0, l)$ is

$$\frac{\rho_0 l^3}{\tau^2} \sim \sum_j B_j Q_j, \tag{12}$$

where B_j are arbitrary dimensionless constants, and the quantities Q_j are some measure of energy in the velocity components. Based on the considerations discussed in § 2.2, we again choose Q_j to be the available kinetic energy of component j, given by (10). We choose to base the determination of time scales on the available kinetic energy of the velocity component parallel to the ODT domain (v_2 in our notation), because eddy events represent motion in this direction. This choice breaks

https://doi.org/10.1017/S0022112001005778 Published online by Cambridge University Press

the symmetry under index exchange only in determining the sequence of events, while maintaining it during the implementation of each individual event. In particular, the quantities B_j are chosen so that the right-hand side of (12) corresponds to the available kinetic energy in component v_2 upon completion of eddy implementation. Based on (8)–(10), this yields

$$\left(\frac{l}{\tau}\right)^2 \sim v_{2,K}^2 + \alpha \sum_j T_{2j} v_{j,K}^2. \tag{13}$$

There is one additional consideration in determining τ. Due to the damping effects of viscosity, any eddy with a time scale much longer than the corresponding viscous time scale $\tau_v \sim l^2/\nu$ for that eddy size should be prohibited. This suggests including a 'viscous penalty' in the relation determining the eddy turnover time, which is therefore recast as

$$\left(\frac{l}{\tau}\right)^2 \sim v_{2,K}^2 + \alpha \sum_j T_{2j} v_{j,K}^2 - Z\frac{\nu^2}{l^2}. \tag{14}$$

The coefficient of proportionality Z in the viscous penalty is an order-unity parameter of the model. For the application considered here, viscosity is irrelevant in the high-Re limit of interest and the inclusion of this cutoff is primarily for convenience in numerical simulation.

The modelling choices leading to (14) are intended to achieve the broadest possible applicability of the model, including extensions to flow phenomena not considered here. For example, consider a flow with a spatially varying v_1 or v_3 profile but v_2 identically zero. The eddy energy as characterized by the right-hand side of (14) can be positive for this case only if the scrambling term (the second term) is large enough to overcome the viscous damping. In this case, the ratio α/Z controls the onset of higher-dimensional motion. This raises the possibility (not yet investigated in detail) that the present formulation may encompass the transition to turbulence as well as fully developed turbulence.

Another possible generalization is the incorporation of buoyancy, with the ODT domain vertically oriented. ODT formulations involving one velocity component have included buoyancy (Kerstein 1999*a*, *b*; Wunsch & Kerstein 2001). The present formulation offers a more detailed representation of buoyancy effects, including both the exchange between gravitational potential energy and vertical kinetic energy and the coupling of this process to the other velocity components by means of the scrambling mechanism.

As in previous versions of ODT, the time scales τ for all possible eddies are translated into an event rate distribution λ, defined as

$$\lambda(y_0, l; t) \equiv \frac{C}{l^2\tau(y_0, l; t)} = \frac{C\nu}{l^4}\sqrt{\left(\frac{v_{2,K}\, l}{\nu}\right)^2 + \alpha \sum_j T_{2j}\left(\frac{v_{j,K}\, l}{\nu}\right)^2 - Z}, \tag{15}$$

where the turnover time based on (14) has been inserted. If the right-hand side of (14) is negative, the eddy is deemed to be suppressed by viscous damping and λ is taken to be zero for that case. In the square-root term of (15), the quantities preceding Z involve groups that have the form of a Reynolds number. Z can be viewed in this context as a parameter controlling the critical Reynolds number for eddy turnover. The relationship between this Reynolds-number threshold and the threshold for transition to turbulence is discussed by Kraichnan (1962).

https://doi.org/10.1017/S0022112001005778 Published online by Cambridge University Press

The foregoing construction of the event rate distribution involves three free parameters: C, α, and Z. The overall rate coefficient C determines the strength of the turbulence in the model; hence it determines the Reynolds number Re or equivalent measures of turbulence intensity. The transfer coefficient α determines the degree of kinetic energy exchange among components. For $\alpha = 0$ (no exchange), this formulation reduces to a specialization of the buoyant stratified flow model of Wunsch & Kerstein (2001) to constant density flows. The viscous cutoff parameter Z determines the smallest eddy size for given local strain conditions. The three parameters in the rate distribution, together with the initial and boundary conditions of the flow being simulated and the physical properties of the fluid (density, viscosity, etc.), constitute the complete set of inputs required by the model.

The sequence of eddies implemented during a simulated realization is sampled from the rate distribution λ. During a time increment $\mathrm{d}t$, the probability of occurrence of an eddy whose location and size are within the ranges $[y_0, y_0 + \mathrm{d}y_0]$ and $[l, l + \mathrm{d}l]$ respectively is $\lambda(y_0, l; t)\,\mathrm{d}y_0\,\mathrm{d}l\,\mathrm{d}t$.

Each event, as well as the viscous evolution (1) between events, changes the velocity profiles v_i and therefore modifies the rate distribution λ. This interaction between the rate distribution and simulated flow evolution is largely responsible for key features of the model such as emulation of the inertial-range turbulent cascade (Kerstein 1999*a*; Wunsch & Kerstein 2001). From a computational viewpoint, it causes explicit construction of, and sampling from, the rate distribution to be unaffordable owing to the need to reconstruct this distribution repeatedly. Instead, an indirect but mathematically equivalent procedure is employed. An alternative rate distribution that remains unchanged during the simulation is specified arbitrarily, though the procedure is most efficient if it approximates the true distribution. Events are sampled from the fixed distribution at fixed time increments. For an event that is sampled at time t, defined by chosen values of y_0 and l, the true value of λ is computed. (The complete procedure for this computation is described in § 2.4.) The true value is then compared to the corresponding value specified by the fixed distribution. The comparison determines an acceptance probability for the event. In the limit of vanishing time increments between samplings, this two-step procedure – random sampling followed by a random trial determining acceptance or rejection – results in an event sequence governed by the true rate distribution, without reconstructing the entire distribution for each sampling operation. Details are provided elsewhere (Kerstein 1999*a*).

2.4. *Large-eddy anomaly*

For time-developing flows, the statistical sampling procedure used in ODT introduces an artifact associated with the occasional selection of an event much larger than the momentum thickness of the flow. These events are rare because the dimensional scalings underlying the method are consistent with scale locality (i.e. events of given size are driven most effectively by forcings of comparable scale). However, the rare large events permitted by the statistical sampling procedure contribute disproportionately to lateral transport, which scales as the square of the event size. Thus, they can dominate the lateral growth of the free shear flows considered here, as well as other flows.

Several ways of mitigating this artifact have been employed previously (Kerstein 1999*a*; Kerstein & Dreeben 2000). Here, a large-eddy suppression mechanism is introduced that is physically motivated, parameter free, and broadly applicable.

To suppress rare large events, the rate λ for a given event is evaluated two different

https://doi.org/10.1017/S0022112001005778 Published online by Cambridge University Press

ways, and the smaller of the two results is used in the sampling procedure outlined in § 2.3. One evaluation is by the method already described in § 2.3, based on (15). The other evaluation involves replacement of each velocity profile $v_i(y,t)$ by a profile that is linear in y, and evaluation of (15) based on these linear profiles. The slope of each profile is taken to be the median value of $|\mathrm{d}v_i/\mathrm{d}y|$ within the eddy range $[y_0, y_0 + l]$.

The key attribute of this procedure is that it assigns a zero rate to any event for which each velocity profile is flat (zero slope) in more than half of the eddy range. Thus, an event encompassing a y interval that is more than twice the width of the active zone of an entraining shear flow is strictly excluded. The median of absolute slope is used in order to avoid a balance of positive and negative values that would result in a zero median for events whose exclusion is not intended. In addition to preventing unphysically large eddies, this procedure reduces the likelihood of events whose available energy is dominated by contributions from a small subinterval of the eddy range. Thus, the procedure further enforces scale locality, which is the conceptual basis of ODT.

The median procedure could be used as a replacement, rather than an augmentation, of the procedure of § 2.3. However, the model is internally most consistent if the true profiles, which must be used in eddy implementation (mapping and energy exchange), are also used in eddy selection. The median procedure as implemented can only reduce the likelihood of a given event, consistent with the objective of excluding certain events with minimal modification of other aspects of the model.

2.5. *Perspective*

In view of the unfamiliar features of the present modelling approach, it is compared briefly to other modelling concepts that have been applied to turbulence. Specifically, the transilient model (Stull 1988), the binary-tree mode-coupling approach, stochastic geometrical constructions, and the wavelet concept are considered.

Stull formulates a one-dimensional turbulence model representing the evolution of a vertical fluid profile in atmospheric turbulence. To capture effects of large-scale motion, he introduces a 'transilient matrix' that prescribes a property transfer rate from any cell of the profile to any other. Matrix coefficients are based on a 'mixing potential' involving production and dissipation terms analogous to those of (14) and a buoyancy term analogous to the ODT formulation of Wunsch & Kerstein (2001). Though there is a resemblance between the dynamical inputs to the two models, kinematically they are quite different. ODT is an unsteady simulation in which fluctuations are inherent and microphysical mechanisms are explicitly represented. Though the transilient model incorporates advective transfers on all length scales (analogous to the incorporation of eddies of all sizes in ODT), it is an ensemble-averaged formulation that does not literally resolve fine-grained structure and evolution.

One could extract rates of eddy-induced cell-to-cell property transfer from ODT simulations and thereby construct the corresponding transilient matrices. This would yield a version of the transilient model that is, in effect, a mean-field representation of ODT advective processes.

The ODT modelling approach is largely motivated by the desire to incorporate multiscale turbulent cascades into a formulation that can address diverse initial-boundary-value problems of interest. The transilient model is an example of an approach that accomplishes the latter but does not model turbulent cascades. If one wishes to do the reverse, namely model cascades but not necessarily couple them to realistic forcing mechanisms, then a lower-dimensional model need not be formulated in physical space. Useful models for this purpose have been formulated that evolve

https://doi.org/10.1017/S0022112001005778 Published online by Cambridge University Press

with respect to a scalar wavenumber k (Fourier-space representation) and time. A cascade model more closely analogous to ODT is the binary-tree mode-coupling approach that evolves in a (1+1)-dimensional ultrametric space, thereby providing a representation of spatial correlations in homogeneous turbulence (Aurell, Dormy & Frick 1997; Benzi *et al.* 1997). Cascade models allow mode interactions to proceed over time. The ODT analogue is the eddy event, which must be instantaneous in order to obtain a physical-space formulation with desired properties. Other turbulence models, such as the randomly forced Burgers equation (Chekhlov & Yakhot 1995) and a one-dimensional Biot-Savart formulation (Constantin, Lax & Majda 1985; De Gregorio 1990), have been formulated in one physical-space dimension, but they do not satisfy the conservation properties necessary for meaningful comparisons to inhomogeneous flows.

Another turbulence modelling approach that has been applied in one dimension is the stochastic construction of one-dimensional functions whose statistical properties resemble turbulent flow properties. Two methods that have been used involve repeated application of a generating function with random selection of function parameters. One method generates the synthetic signal by additive superposition (Juneja *et al.* 1994), analogous in some respects to the role of the kernel in ODT. The other (Vicsek & Barabási 1991) involves a recursive refinement process that is analogous to the multiplicative increase of property gradients by the triplet map. Both ODT and the stochastic constructions involve the specification of generators (functions in the constructions; both a kernel function and a mapping in ODT) whose repeated application involves random parameter selection. The key difference is that ODT is a dynamical time-evolving model in which each selection step depends on past history.

The kernel $K(y)$ that is used both to measure available energy and to implement energy transfers may be viewed as a wavelet construct. Like a wavelet, the kernel is effectively a local filter that selects fluctuations whose length scales are comparable to the eddy size l. It thus enforces the correspondence between the eddy size and the scale of the dynamics governing its occurrence. This may be regarded as a matter of definition rather than a physical principle, because the turbulent eddy is a concept rather than a physical observable; it is analogous to a normal mode of a linear system, but has no precise definition owing to the strong nonlinearity of the Navier–Stokes equations. If a turbulent eddy is heuristically defined as motion in response to local forcing at a given length scale, then the use of a wavelet-type construct to characterize the forcing can be viewed as a consistency requirement rather than a physical modelling assumption.

3. Application to free shear flows

3.1. *Numerical implementation and features of the simulations*

For each of the flow configurations considered here, computed results are based on 5000 simulated realizations. To facilitate initial transient relaxation, it is convenient to choose the initial velocity profiles to be continuous functions of y. Accordingly, the initial v_1 profile for the mixing layer is a linear ramp between two semi-infinite flat regions whose velocity difference is denoted ΔU. The initial v_1 profile for the wake is a symmetric tent. The initial v_2 and v_3 profiles for both flows are nominally zero, but are seeded with small random perturbations as explained in § 2.2. For both flows, the computational domain is taken to be large enough so that it is effectively infinite, i.e. the turbulent region does not extend close enough to the boundaries during the simulations to be affected by their presence.

https://doi.org/10.1017/S0022112001005778 Published online by Cambridge University Press

Owing to the coordinate invariance of the pressure-scrambling mechanism (§ 2.2), the statistical evolution of velocity components subject to the same initial and boundary conditions (in this instance, the v_2- and v_3-components) is indistinguishable in the present formulation. A more general formulation that breaks this symmetry while maintaining required invariance properties has been formulated and tested. This formulation involves three eddy types, each of which allows energy exchange between two of the three velocity components. Because eddy selection is based on the v_2-component available kinetic energy (§ 2.3), this generalization breaks the (v_2, v_3) symmetry. In particular, it captures the two-dimensional (v_1, v_2) character of the dominant shear instabilities. However, this formulation is not adopted here because its performance is not commensurate with the additional complexity and parameter tuning that it entails. The formulation used here is intended to capture the principal manifestation of anisotropy, resulting from the imposition of the initial shear solely on the v_1-component, but not the secondary manifestations that break (v_2, v_3) symmetry.

The present focus is the self-similar evolution of flow statistics seen in high-*Re* DNS. The ODT simulations exhibit analogous high-*Re* self-similarity.

The wake results reported here correspond to Reynolds number, defined as $Re = (1/\nu)\int_{-\infty}^{\infty}\langle v_1\rangle\,\mathrm{d}y$, equal to 2000, the same value as in the DNS comparison case. In the time-developing wake, *Re* remains constant during the simulations. Additional runs for other *Re* values indicate that this value of *Re* is high enough so that flow statistics for the self-similar flow regime are insensitive to *Re*.

For the mixing layer, the initial value of *Re* based on ΔU and the momentum thickness $\delta_m = \int_{-\infty}^{\infty}[\frac{1}{4} - (\langle v_1\rangle/\Delta U)^2]\,\mathrm{d}y$ is 427, compared to an initial DNS value of 800. (The definition of δ_m is based on nominal v_1 values of $\pm\Delta U/2$ in the flat regions.) For this flow, *Re* increases with time, so the onset of self-similar evolution is inherently a confirmation of *Re* insensitivity.

The lack of *Re* sensitivity for both flows implies that features of the model associated with viscous transport are negligible for the *Re* values considered. This implies insensitivity not only to the kinematic viscosity ν, but also to the model parameter Z that controls the strength of the viscous penalty in the eddy rate distribution, (15). This insensitivity has been verified by running representative cases for different values of Z. The results presented here correspond to $Z = 0.02$.

As noted in § 2.2, the allowed range of the model parameter α controlling the degree of energy exchange among velocity components is [0,1], where $\alpha = 0$ corresponds to no exchange and hence no representation of pressure scrambling. Simulations have been performed for $\alpha = \frac{1}{3}$, $\frac{2}{3}$, and 1. The case $\alpha = 1$ maximizes the intercomponent exchange, an interesting limit to consider. Based on (8)–(10), $\alpha = \frac{2}{3}$ corresponds to equalization of the component available energies. This is consistent with the intuitive notion that an eddy turnover erases memory of fluid orientation in any fixed reference frame, implying no dependence of the post-eddy distribution of available energy among velocity components on the distribution prior to the turnover.

It is found that results for $\alpha = 1$ are in best agreement with DNS results, so most of the results presented here correspond to this 'maximum exchange' (M) case. To illustrate the sensitivity to α, some results are also presented for the 'equipartition' (E) case, $\alpha = \frac{2}{3}$. Implications with regard to the physical interpretation of the model are noted in § 4. We remark here that any α within the allowed range results in an overall tendency to equalize the component available energies, so the model is generally consistent with the 'return-to-isotropy' concept that is the basis of pressure–strain modelling in closure-based models (Pope 2000).

https://doi.org/10.1017/S0022112001005778 Published online by Cambridge University Press

The model parameter C is an overall rescaling of the event rate distribution. In flow regimes that are insensitive to the strength of viscous processes, eddy events entirely control flow development, so rescaling of the eddy event rate is equivalent to rescaling of the time coordinate, and hence rescaling of the growth rate. For the self-similar regimes of both flows considered here, it has been verified that variation of C changes only the growth rate, with no effect on other properties other than proportionate rescaling of quantities dependent on the growth rate.

These self-similar regimes exhibit the same growth laws as the corresponding DNS results. The numerical coefficients in the DNS growth laws, $(1/\Delta U)\mathrm{d}\delta_m/\mathrm{d}t = 0.014$ for the mixing layer and $(1/U_0)\mathrm{d}b/\mathrm{d}t = 0.12$ for the wake (where b is the full width at half-maximum of the mean velocity profile, growing as $t^{1/2}$, and U_0 is the centreline mean velocity, decaying as $t^{-1/2}$), are matched for $C = 3.78$ and 5.55 for the mixing layer and wake, respectively. These C values were used for all α values considered because the growth rates were found to be insensitive to α.

For each of the flow statistics considered, the onset of self-similarity was demonstrated by verifying the collapse of normalized quantities computed within time bands. Once the self-similar time regime was identified, all the normalized data within the self-similar regime were pooled. This procedure was applied to all the results that are presented here.

Figure 1 illustrates some features of the simulation. For the mixing layer and the wake, respectively, the eddy events during a simulated realization are represented by vertical line segments. The horizontal location of each segment corresponds to the time of occurrence of the event, and the vertical extent of the segment corresponds to the eddy interval.

For both flows, it is evident that the width of the turbulent zone grows primarily by the occurrence of an occasional event that causes a large increase, with some additional contribution by the more numerous small events. This process is consistent with the dominant role of large engulfing motions and the secondary role of persistent small-scale nibbling in turbulent entraining flows. The relative contributions of these mechanisms in the simulations are sensitive to the method that is used to prevent a large-eddy anomaly (§ 2.4). It would be of interest to quantify these contributions and compare them to measurements, but this is not attempted here.

Also evident in both flows is bunching of events, particularly after the occurrence of a large event. This reflects feedback processes that induce the model analogue of the turbulent cascade (§ 2.3). Based on the defined measure of available energy, wrinkling of velocity component profiles by a triplet map increases the likelihood of subsequent smaller events in its vicinity. This mechanism accounts for both the cascade of velocity fluctuations to smaller scales in the simulation and the bunching of eddies, analogous to turbulence intermittency.

Figure 1 also highlights the connection between large-scale forcing and small-scale flow structure. Owing to the velocity difference maintained across the mixing layer, the flow Reynolds number increases in proportion to the width of the turbulent zone. The Kolmogorov inertial-range scalings therefore imply that the size of the smallest eddies scales as the $\frac{1}{4}$-power of the width, and that their turnover time scales as the $\frac{1}{2}$-power of the width. The wake, however, is a constant-Re flow, so the small eddies scale in the same manner as the large eddies. Accordingly, their size scales as the turbulent zone width and their turnover time scales as the square of the width. The eddy sequences shown in figure 1 appear to be broadly consistent with these scalings.

https://doi.org/10.1017/S0022112001005778 Published online by Cambridge University Press

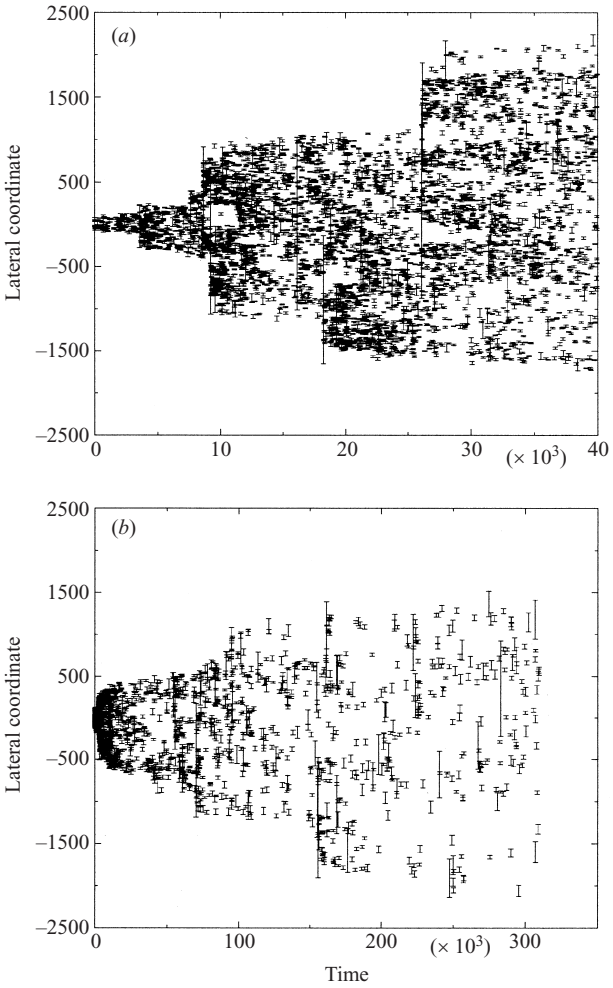

FIGURE 1. Eddy locations (vertical line segments) versus time in one simulated realization (case M) of (*a*) the planar mixing layer, (*b*) the planar wake. Spatial units are $20\nu/\hat{U}$ and time units are $20\nu/\hat{U}^2$, where $\hat{U}$ denotes ΔU for the mixing layer and the initial value of U_0 for the wake.

3.2. *Comparison to direct numerical simulations*

Lateral profiles of mean velocity, Reynolds shear stress, velocity fluctuations, and velocity fluctuation budgets obtained from the self-similar regime of the ODT simulations are compared to DNS results. All flow properties are normalized as in the DNS studies. Lengths are scaled by δ_m and b, and velocities are scaled by ΔU and U_0, for the mixing layer and wake, respectively. Probability density functions (PDFs) and related properties of a passive advected scalar are also examined.

Figures 2 and 3 show that maximum exchange (M) yields reasonable agreement with the DNS mean axial velocity and Reynolds shear stress profiles of both flows. Equipartition (E) results closely resemble those for case M. The shapes of these profiles are largely dictated by the mean spreading rate. ODT spreading rates have been matched to the DNS spreading rates for these flows by parameter adjustment (§ 3.1), so these comparisons are not stringent tests of model performance.

As noted in § 2.1, advection on the one-dimensional domain is implemented in ODT

https://doi.org/10.1017/S0022112001005778 Published online by Cambridge University Press

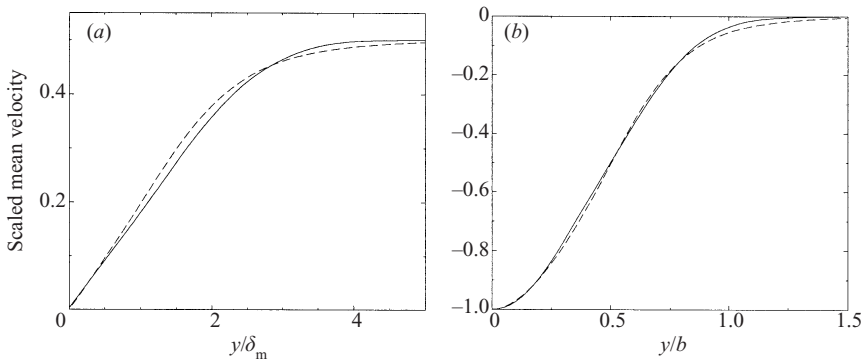

FIGURE 2. Lateral profile of mean streamwise velocity, scaled by ΔU for the mixing layer and by U_0 for the wake: – – –, ODT case M; ——, DNS. (*a*) Mixing layer. (*b*) Wake.

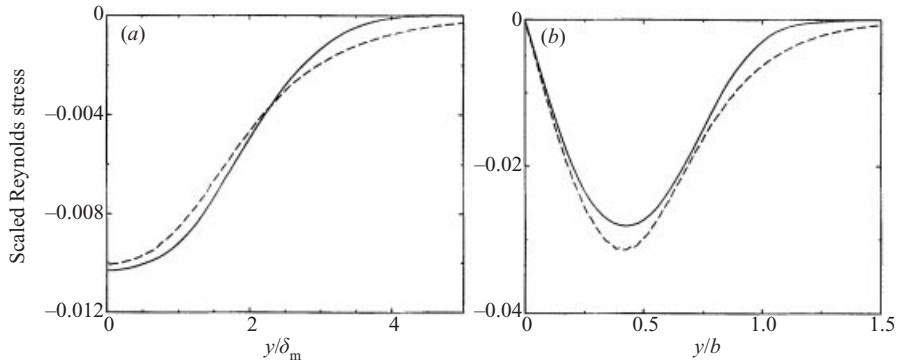

FIGURE 3. Lateral profile of Reynolds shear stress $\langle v_1' v_2' \rangle$, scaled by $(\Delta U)^2$ for the mixing layer and by U_0^2 for the wake: – – –, ODT case M; ——, DNS. (*a*) Mixing layer. (*b*) Wake.

as a sequence of instantaneous events rather than as continuous motion governed by the velocity profiles. Therefore the flux interpretation of quantities such as the Reynolds stress component $\langle v_1' v_2' \rangle$ is not applicable if these quantities are computed in ODT directly from the velocity components. In Navier–Stokes flow, $\langle v_1' v_2' \rangle$ can be interpreted as the advection of v_1 fluctuations by v_2 fluctuations, but in ODT, the v_2 velocity does not directly prescribe the advection of v_1 (or of any other fluid property). Therefore the Reynolds stresses and other advective fluxes (arising, e.g., in velocity fluctuation budgets) are evaluated in ODT by monitoring eddy-induced fluxes during simulated realizations. This assures that conservation laws and balance equations are satisfied exactly. The formal development of this approach is presented in the Appendix.

Lateral profiles of ODT velocity-component variances $\langle v_1'^2 \rangle$, $\langle v_2'^2 \rangle$, and $\langle v_3'^2 \rangle$, and their sum q^2, are compared to DNS results in figure 4. As explained in § 3.1, ODT simulations of the flows considered here do not distinguish between the v_2 and v_3 velocity components, so all statistical properties of these two components that are shown in the figures are identical. The DNS results indicate that the differences between the statistics of these components are smaller than the differences between either of them and the v_1-component statistics. This is consistent with the physical origins of the anisotropy, discussed in § 3.1.

It would be expected that the difference between cases E and M would affect the

https://doi.org/10.1017/S0022112001005778 Published online by Cambridge University Press

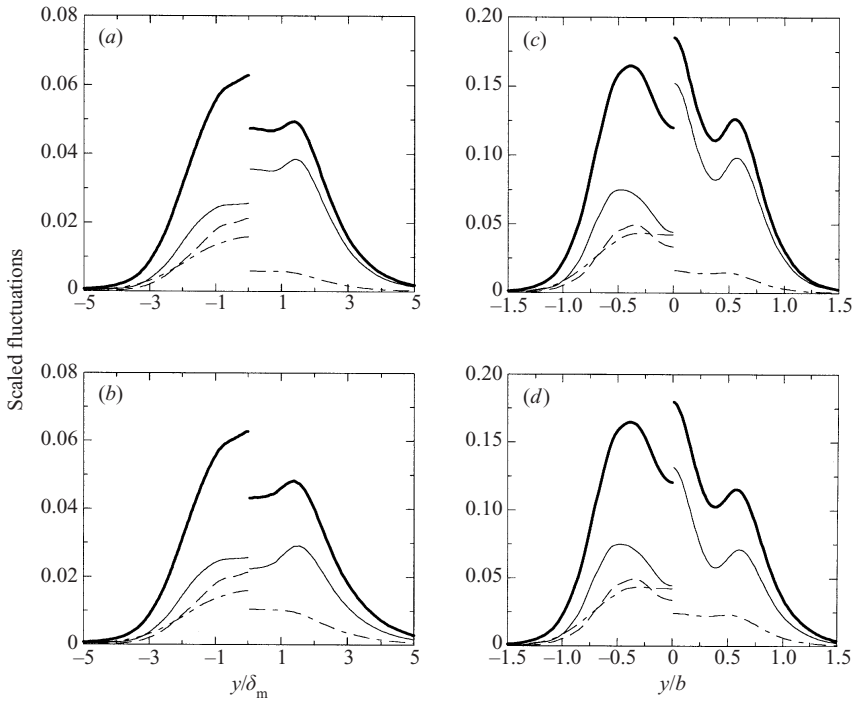

FIGURE 4. Lateral profiles: —, q^2; ——, $\langle v_1'^2\rangle$; —·—, $\langle v_2'^2\rangle$; – – –, $\langle v_3'^2\rangle$, scaled by $(\Delta U)^2$ for the mixing layer and by U_0^2 for the wake. (The ODT $\langle v_3'^2\rangle$ profiles are identical to the ODT $\langle v_2'^2\rangle$ profiles.) ODT and DNS results are plotted right and left of centreline, respectively. (*a*) Mixing layer, case E. (*b*) Mixing layer, case M. (*c*) Wake, case E. (*d*) Wake, case M.

distribution of total variance q^2 between the v_1-component and the other (identical) components more than it would affect q^2 itself. The computed results are consistent with this expectation. Both formulations transfer less variance from v_1 to the other components than indicated by the DNS. Therefore case M, in which the transfer is maximal within the ODT framework, is in better agreement with DNS component variances.

The overall height and width of the ODT q^2 profiles agree reasonably well with their DNS counterparts, although significant differences in profile shape are apparent. Thus, ODT provides a reasonable overall representation of the total turbulent kinetic energy in these flows, irrespective of the details of the scrambling mechanism in the model.

Figures 5–8 compare ODT and DNS budgets of $\langle v_1'^2\rangle$, $\langle v_2'^2\rangle$, $\langle v_3'^2\rangle$, and q^2, respectively. (The definitions and ODT representations of the terms of these budgets are discussed in the Appendix.) The most significant difference between the results for the two ODT cases is the better agreement of case M with the DNS budgets of $\langle v_2'^2\rangle$ and $\langle v_3'^2\rangle$. This is not surprising in view of the better distribution of q^2 among velocity components that is obtained for case M. Likewise, the case-M budgets of $\langle v_1'^2\rangle$ for both flows are closer to the corresponding DNS budgets than are the case-E budgets.

As expected, the q^2 budgets are least sensitive to the choice of formulation. Wake simulations for $\alpha = \frac{1}{3}$ (not shown) yield significantly different budgets of q^2 and of velocity-component variances. Reduction of α must eventually affect turbulence energetics because fluctuations are suppressed entirely in the limit of vanishing α. However, there appears to be little sensitivity to α at higher α values. Collectively, the

https://doi.org/10.1017/S0022112001005778 Published online by Cambridge University Press

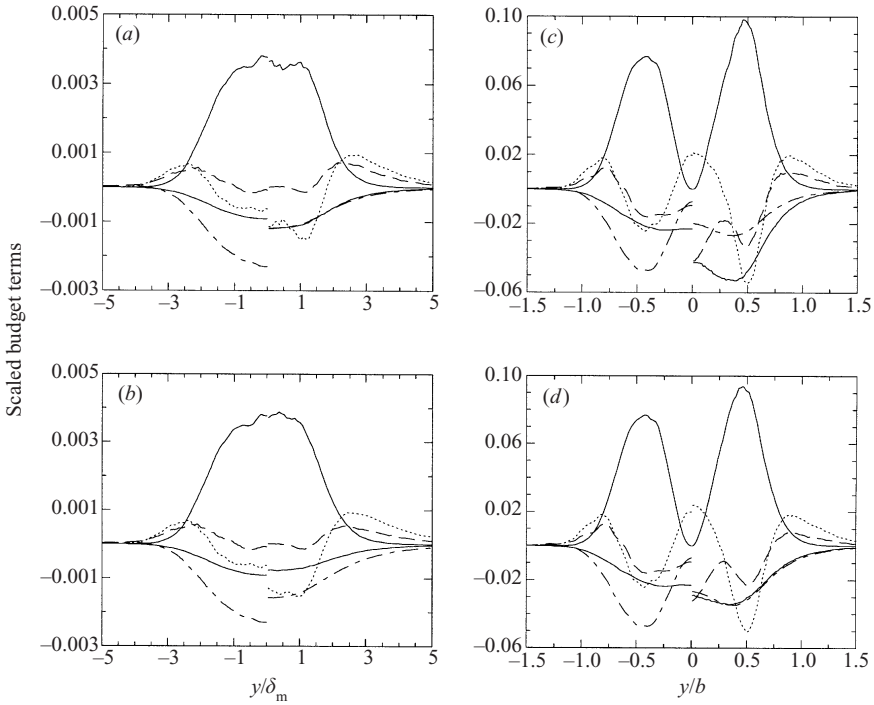

FIGURE 5. Budget of $\langle v_1'^2 \rangle$, scaled by $\Delta U^3/\delta_m$ for the mixing layer and by U_0^3/b for the wake: ——, production (upper), dissipation (lower); — — —, time derivative; ·····, advective transport; —·—, scrambling. ODT and DNS results are plotted right and left of centreline, respectively. (*a*) Mixing layer, case E. (*b*) Mixing layer, case M. (*c*) Wake, case E. (*d*) Wake, case M.

comparisons between ODT and DNS indicate that the model provides a reasonable quantitative representation of turbulent free shear flow energetics.

Comparable performance, but more limited in scope, was obtained previously using a scalar velocity formulation (Kerstein & Dreeben 2000). One noticeable difference between the present and previous results is the shape of predicted q^2 and $\langle v_1'^2 \rangle$ profiles for the wake. The previous study showed less prominent variations of profile slope than indicated by the DNS, but the present results (figures 4*c* and 4*d*) show more prominent variations. This may be related to the deep minimum of the advective transport term of the $\langle v_1'^2 \rangle$ budget (figures 5*c* and 5*d*); the scalar velocity formulation predicts a shallower minimum than indicated by the DNS. With regard to v_1 statistics, the difference between the two formulations is kernel implementation that represents pressure scrambling, but also affects transport of velocity fluctuations and thus the velocity fluctuation profiles (see the Appendix). It is reasonable that the wake would be more affected than the mixing layer because the mixing layer has a broader turbulence production zone, so effects specific to the shape of the kernel function should be smeared to a greater extent in the mixing layer. Figure 1 indicates the relatively uniform distribution of eddy events within the mixing layer, as would be expected.

ODT is distinct in character from other statistical models of turbulence in that it is a fully resolved unsteady simulation and accordingly, can predict additional statistical properties with no further empirical input. To illustrate this, a passive scalar has been included in the ODT simulations in order to obtain families of scalar

https://doi.org/10.1017/S0022112001005778 Published online by Cambridge University Press

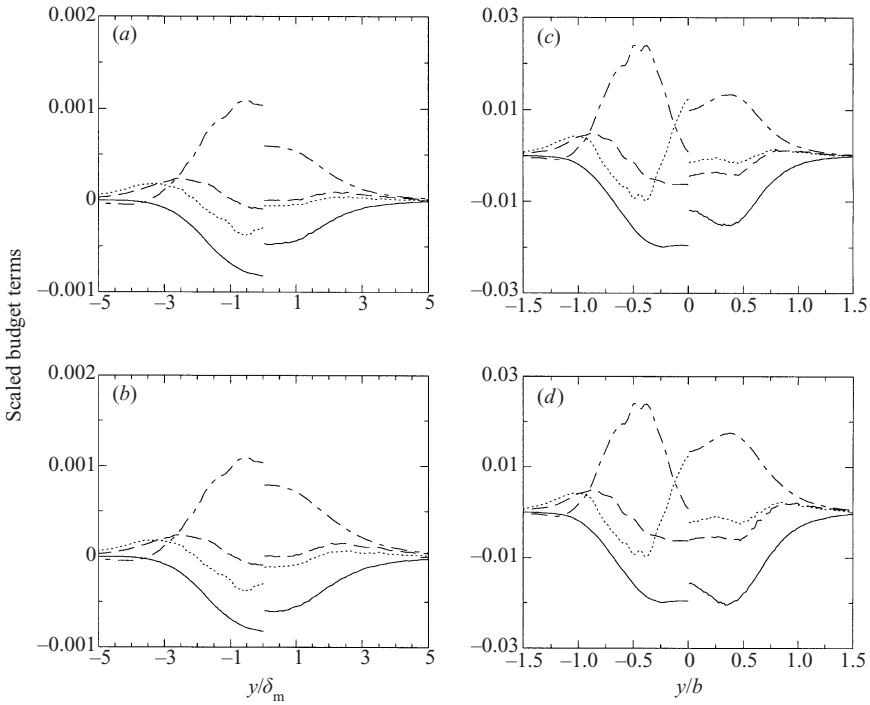

FIGURE 6. Budget of $\langle v_2'^2 \rangle$. Format as in figure 5. (*a*) Mixing layer, case E. (*b*) Mixing layer, case M. (*c*) Wake, case E. (*d*) Wake, case M.

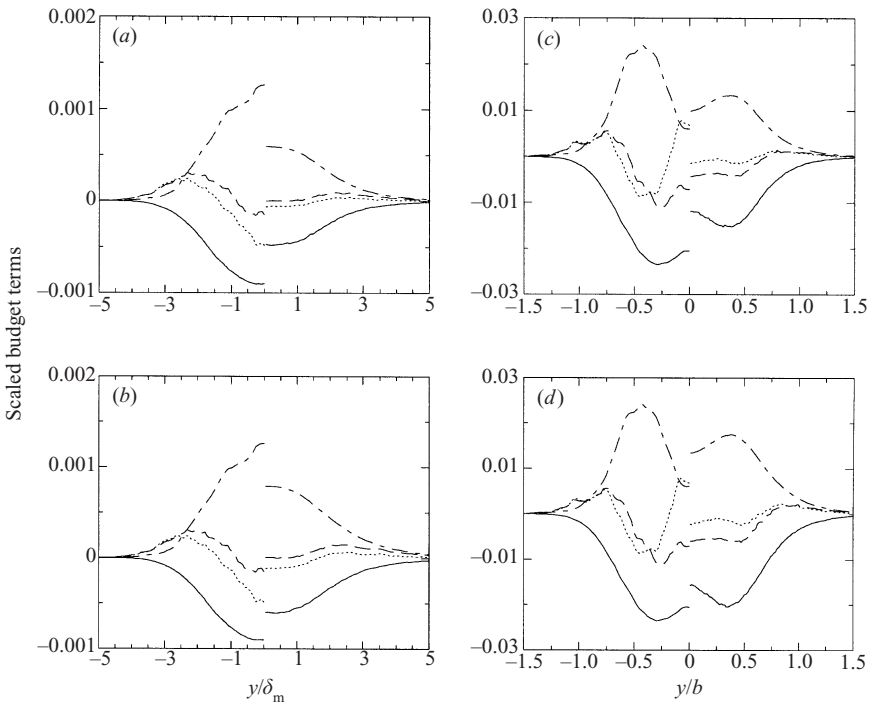

FIGURE 7. Budget of $\langle v_3'^2 \rangle$. Format as in figure 5. (*a*) Mixing layer, case E. (*b*) Mixing layer, case M. (*c*) Wake, case E. (*d*) Wake, case M.

https://doi.org/10.1017/S0022112001005778 Published online by Cambridge University Press

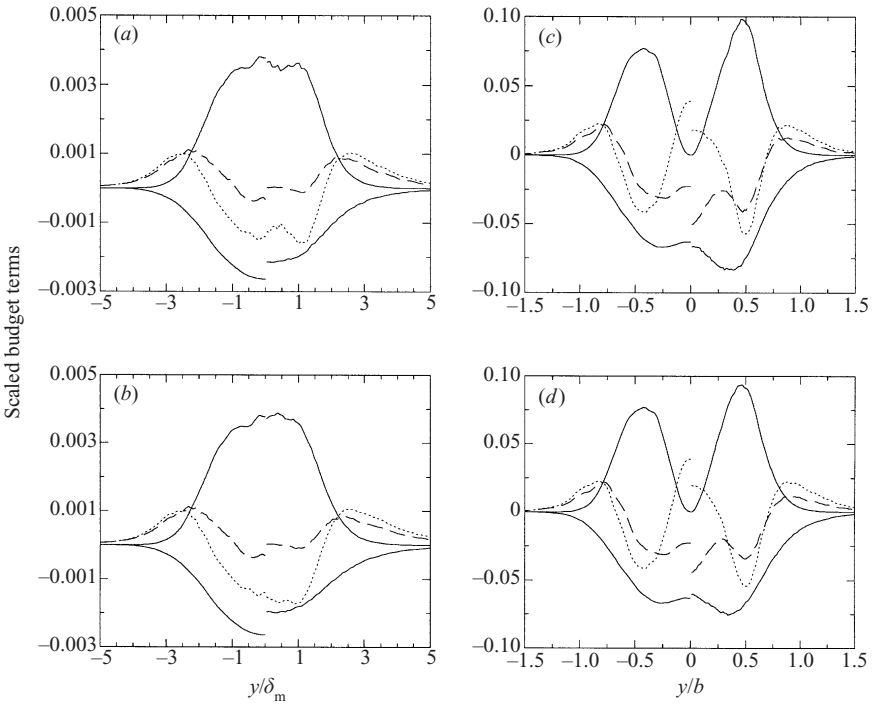

FIGURE 8. Budget of q^2. Format as in figure 5. (*a*) Mixing layer, case E. (*b*) Mixing layer, case M. (*c*) Wake, case E. (*d*) Wake, case M.

PDFs parameterized by normalized lateral location. The ODT results are compared to DNS results (Rogers & Moser 1994, plus additional unpublished data provided by the authors). For both flows, $Sc = 0.7$ for the passive scalar (Mike Rogers, personal communication; a different value is stated is the cited reference).

For both flows, the initial scalar profile $\theta(y,0)$ is constant on either side of the mixed zone, with values 0 and 1. As in the initialization of v_1, a linear ramp is introduced between the constant regions to facilitate transient relaxation.

The ODT results for cases E and M do not differ significantly, so only case M results are shown. Introducing a scalar thickness $\delta_s = \int \theta(1-\theta)\,\mathrm{d}y$, ODT values of the ratios δ_s/δ_m (for the mixing layer) and δ_s/b (for the wake) are found to differ by up to 20% from DNS values. To compare scalar PDFs on a consistent basis, lateral location is parameterized by $\hat{y} \equiv y/\delta_s$.

ODT and DNS scalar mean and variance profiles, plotted versus $\hat{y}$, are shown in figures 9 and 10. These and all other scalar statistics correspond to the regime of self-similar scalar evolution for both ODT and DNS. ODT provides a reasonable overall representation of the DNS profiles, though there are some significant differences.

ODT and DNS scalar PDFs are compared in figure 11. For both flows, the ODT results are closest to DNS results for relatively well-mixed conditions. This applies to the centreline ($\hat{y} = 0$) PDFs and to most of the other PDFs for $\theta < 0.7$. PDFs are shown only for $\hat{y} \geqslant 0$ because they are invariant under the transformation $\hat{y} \to -\hat{y}$, $\theta \to 1-\theta$. $\theta = 1$ corresponds to the positive-$\hat{y}$ free-stream value, so the large-θ side of positive-$\hat{y}$ PDFs reflects a relatively strong contribution from newly entrained free-stream fluid that is not yet very well mixed. The entrainment-sensitive portions

https://doi.org/10.1017/S0022112001005778 Published online by Cambridge University Press

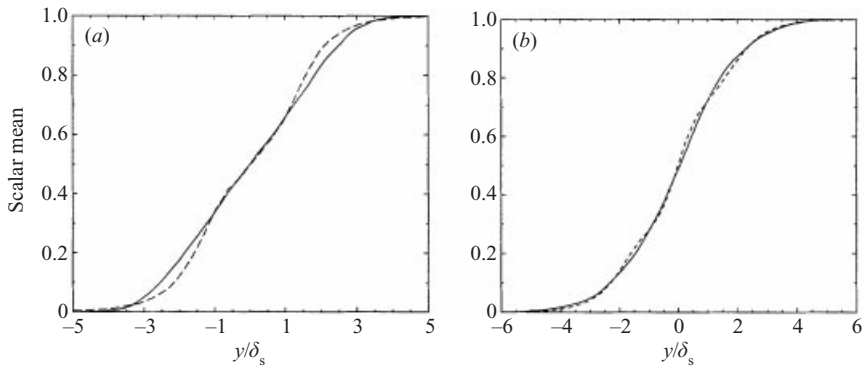

FIGURE 9. Passive scalar mean profile, plotted versus lateral location y scaled by the scalar thickness δ_s. – – –, ODT case M; ——, DNS. (*a*) Mixing layer. (*b*) Wake.

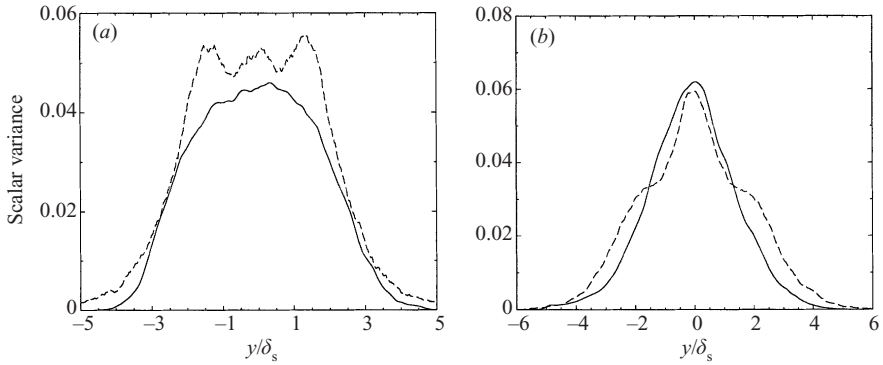

FIGURE 10. Passive scalar variance profile. Format as in figure 9. – – –, ODT case M; ——, DNS. (*a*) Mixing layer. (*b*) Wake.

of the PDFs are not well represented by ODT because the model does not capture the flow-specific three-dimensional structure of the large entraining eddies.

4. Discussion

The goal of the successive stages of development of ODT (Kerstein 1999*a*; Wunsch & Kerstein 2001) is to achieve as complete and precise an emulation of Navier–Stokes turbulence as possible on a one-dimensional spatial domain. In this study, two related features of Navier–Stokes turbulence are incorporated: the three-dimensional vector character of the velocity field, and the consequent intercomponent energy transfer in response to pressure fluctuations. In addition, a large-eddy regulation mechanism is introduced that is more robust than mechanisms used previously.

Intercomponent energy transfer is implemented by applying the return-to-isotropy concept to individual eddies, in contrast to its application to averaged quantities in second-order closure models. The new method is based on eddy-resolved evaluation of the transferrable energy in each velocity component based on an available-energy construct.

The prescription of the redistribution of this energy among the components is not unique, but coordinate invariance and physical intuition identify two preferred options. One is based on the assumption that the individual eddy causes loss of

https://doi.org/10.1017/S0022112001005778 Published online by Cambridge University Press

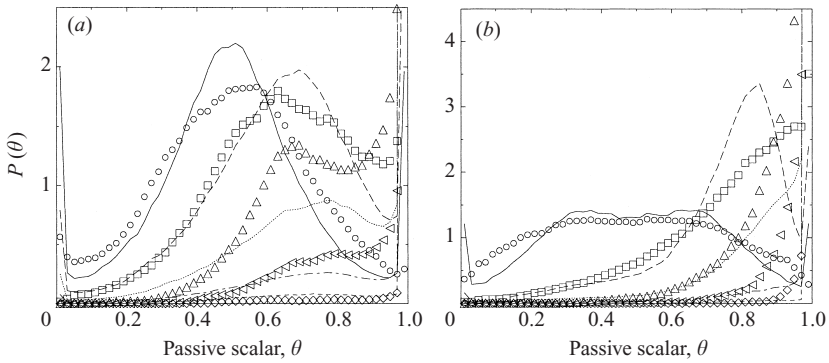

FIGURE 11. Passive scalar probability density: ODT case M (lines) and DNS (symbols). (*a*) Mixing layer: $y/\delta_s = 0$ (——, ○), 1.0 (— — —, □), 2.0 (· · · · · ·, △), 3.0 (— · —, ◁), 4.0 (- - - -, ◇). (*b*) Wake: same format, but for $y/\delta_s = 0$, 1.25, 2.5, 3.75, and 5.0, respectively.

directional preference, and thus equipartition of the available energy among the three velocity components (case E). The other maximizes the overall energy transfer rate from the high-energy to the low-energy velocity components, thus maximizing the rate of return to isotropy in flows with unequal turbulent-kinetic-energy production rates for different components (case M).

In applications to free shear flows, it is found that neither method transfers as much turbulent kinetic energy from the shear-driven velocity component, v_1, to the other components as indicated by DNS results, so case M is more accurate in this regard because it maximizes the transfer. It would be interesting to investigate whether Navier–Stokes turbulence likewise maximizes intercomponent transfer subject to physical constraints.

One implication is that the interpretation of the triplet map as an individual turbulent eddy may be too literal. Such a literal interpretation would be questionable regardless of the physical realism of the model because a turbulent eddy in the most general context (i.e. not referring specifically to large-scale flow structures or dissipation-scale vortices) is an idealization rather than an identifiable motion in turbulent flow. Case-E energy transfer is motivated by the interpretation of the triplet map as a representation of a vortical overturn that erases memory of the prior orientation of the velocity vector. Case M implies a more subtle interpretation in which the scaling properties governing the ensemble of eddy events are more fundamental than the relationship between individual events and individual fluid motions. Indeed, it has been proposed that the robustness of the scalings that determine the time scales of individual events in the simulation is the main reason for the breadth of predictive capability exhibited by ODT (Kerstein 1999*a*).

A practical feature of the vector formulation of ODT is that it may facilitate the use of the model as a subgrid momentum closure for large-eddy simulation (LES) of turbulence. An effort to implement ODT as a near-wall submodel for LES has been initiated (Kerstein *et al.* 2001).

The vector formulation also offers the possibility of simulating rotating flow by taking $i = 3$ to be the azimuthal coordinate in a cylindrical coordinate system. Equations (1) and (2) would be modified accordingly, and centrifugal acceleration could be incorporated much as the gravitational acceleration in buoyant flow applications (Wunsch & Kerstein 2001). It would be interesting to test the ODT treatment of this particularly challenging problem.

https://doi.org/10.1017/S0022112001005778 Published online by Cambridge University Press

Additional opportunities for extensions are provided by the energy transfer mechanism that was introduced here in the context of energy redistribution among velocity components. This mechanism played a key role in a recent application of ODT to buoyant stratified flow (Wunsch & Kerstein 2001). It may likewise enable applications to compressible flow (by coupling flow energetics to the energy equation), multiphase flow (e.g. a dispersed phase with two-way coupling or immiscible fluids with significant surface-tension energy), and magnetohydrodynamics. Also, it has been noted that the present framework may enable a quantitative representation of the transition to turbulence.

Thus, the formulation introduced here enables systematic extension of ODT to many challenging turbulent flow regimes. Tests of the validity of ODT in these contexts would provide further indications of the robustness of the modelling approach.

The authors would like to thank R. D. Moser and M. M. Rogers for providing numerical results from their publications and from unpublished work. This research was supported by the Division of Chemical Sciences, Geosciences & Biosciences, Office of Basic Energy Sciences, US Department of Energy.

Appendix. Statistical properties of flow realizations

ODT is formulated as a closed system on a one-dimensional domain. The model can be viewed as a simulation of a one-dimensional line of sight in a three-dimensional flow. However, such a line of sight is not a closed system. Modeling it as a closed system is an artifact that may be the cause of some of the discrepancies between model predictions and measured turbulence properties. However, it is unlikely that this is the most severe approximation within the model.

A key benefit of taking the one-dimensional domain to be a closed system is that conservation laws can be enforced. The measure-preserving property of the triplet map enforces conservation of mass. In fact, this property assures that the triplet map conserves all domain-integrated quantities, including velocity moments of all orders. The pressure-scrambling mechanism is formulated so as to conserve momentum and total energy while redistributing energy among velocity components. Viscous dissipation, implemented in a conventional manner, removes kinetic energy while conserving momentum.

Accordingly, momentum and energy budgets can be formulated for ODT that are broadly analogous to the usual relations based on the Navier–Stokes equations. Here, ODT budgets relevant to the present application are formulated, both to refine the analogy to Navier–Stokes turbulence and to provide operational definitions of relevant flow statistics.

For this purpose, a notional instantaneous evolution equation is written for ODT as follows:

$$\frac{\partial v_i}{\partial t} = \nu \frac{\partial^2 v_i}{\partial y^2} + M_i + K_i. \tag{A 1}$$

This equation formally represents the three processes that can change the value of v_i at a given location y and time t. The viscous term has its usual form. M_i and K_i represent changes induced by triplet-map and pressure-scrambling operations, respectively. For example, if a triplet map at time t_0 replaces the v_i value at given y, denoted $\hat{v}_i$, by a new value $\tilde{v}_i$, then $M_i(y,t) = (\tilde{v}_i - \hat{v}_i)\delta(t - t_0)$. The formal definition of K_i is analogous, with $\hat{v}_i$ and $\tilde{v}_i$ now evaluated before and after the pressure-scrambling operation. Numerical implementation of statistical data analysis is based on ensemble-averaged equations derived from (A 1).

https://doi.org/10.1017/S0022112001005778 Published online by Cambridge University Press

Before averaging (A 1), the role of K_i in the context of momentum and energy balances is considered. Though kernel addition during eddy implementation is intended to incorporate pressure-scrambling effects, this operation may be interpreted formally as a combination of scrambling and transport contributions to balance equations. In particular, a given kernel-induced change $K_i(y,t)$ may reflect momentum and energy transfers to other velocity components (scrambling) and/or to the same velocity component at other spatial locations (transport). Accordingly, K_i is expressed as a sum, $K_i = S_i + T_i$, of scrambling and transport contributions.

The kernel K is required to obey $\int K\,\mathrm{d}y = 0$ so that the pressure-scrambling operation conserves momentum. Accordingly, for a given eddy $\int K_i\,\mathrm{d}y = 0$. The transport contribution T_i should be defined so that its integral is zero, because it represents i-component momentum transfer along the y-coordinate and therefore is not a net momentum source or sink for this component. These integral constraints are satisfied only if $\int S_i\,\mathrm{d}y = 0$.

The latter result does not uniquely define S_i, but the choice $S_i \equiv 0$ is clearly preferred because it corresponds to the absence of a pressure-scrambling contribution to the ODT mean momentum equation, in accordance with the absence of pressure scrambling in the Navier–Stokes mean momentum equation. In fact, this equation lacks any pressure-fluctuation terms, so T_i should not be regarded as a pressure-transport contribution. Rather, M_i and T_i together determine the ODT analogue of mean advective transport.

The ODT mean momentum equation is obtained by taking the ensemble average of (A 1). Substituting T_i for K_i, this gives

$$\frac{\partial}{\partial t}\langle v_i\rangle = \nu\frac{\partial^2}{\partial y^2}\langle v_i\rangle + \langle M_i\rangle + \langle T_i\rangle, \tag{A 2}$$

which may be compared to the constant-density Navier–Stokes mean momentum equation for planar time-developing flow (Moser *et al.* 1998),

$$\frac{\partial}{\partial t}\langle v_1\rangle = \nu\frac{\partial^2}{\partial y^2}\langle v_1\rangle - \frac{\partial}{\partial y}\langle v_1'v_2'\rangle, \tag{A 3}$$

where $v_i' \equiv v_i - \langle v_i\rangle$. (Owing to planar symmetry, $\langle v_2\rangle$ and $\langle v_3\rangle$ are identically zero.) The comparison identifies the ODT analogue of the Reynolds-stress component $\langle v_1'v_2'\rangle$ for this class of flows. Owing to the finite lateral extent of the turbulent zone, $\langle v_1'v_2'\rangle = 0$ at $y = \infty$, so at any location y^*, (A 2) and (A 3) give

$$\langle v_1'(y^*)v_2'(y^*)\rangle = \int_{y^*}^{\infty}\mathrm{d}y(\langle M_1\rangle + \langle T_1\rangle) \equiv I_1(y^*). \tag{A 4}$$

The notation $I_i(y^*)$ is introduced in order to distinguish the operational evaluation of $\langle v_i'(y^*)v_2'(y^*)\rangle$ in ODT from the conventional Navier–Stokes definition of this quantity. (Generalization of the derivation of (A 4) to $i \neq 1$ is straightforward.)

Equation (A 3) is consistent with the physical interpretation that $\langle v_1'(y^*)v_2'(y^*)\rangle$ represents the rate of increase of $\int_{y^*}^{\infty}\mathrm{d}y\langle v_1(y)\rangle$ due to turbulent transfer of the v_1 velocity component across $y = y^*$. The terms on the right-hand side of (A 4) are the contributions of the ODT turbulent transfer mechanisms to this integral.

Operationally, these contributions are evaluated by gathering statistics from ODT realizations in finite time bins. Omitting for now the viscous contribution, (A 2) implies that the mean velocity increment over a time increment Δt is

$$\langle \Delta v_1\rangle = \langle M_1\Delta t\rangle + \langle T_1\Delta t\rangle, \tag{A 5}$$

https://doi.org/10.1017/S0022112001005778 Published online by Cambridge University Press

where $M_1\Delta t$ and $T_1\Delta t$ are determined, for a given realization, by summing the respective Δv_1 contributions over all eddies occurring during the designated time interval. This summation is performed separately at each location y, though the y-argument has been suppressed in the analysis. An average of these contributions over an ensemble of realizations yields $\langle \Delta v_1 \rangle$. Dividing by Δt, a discrete-time estimate of the advective terms on the right-hand side of (A 2), specialized to $i = 1$, is obtained. Substitution into (A 4) then yields the ODT analogue of $\langle v_1' v_2' \rangle$.

As noted in § 3.2, this result is different from what would be obtained by evaluating $\langle v_1' v_2' \rangle$ based on ODT velocity profiles v_1 and v_2. ODT velocities do not literally advect fluid, so their use in this way would not be physically meaningful. However, ODT is formulated so that energetics based on these profiles are meaningful. In particular, budgets of the component contributions, $\frac{1}{2}\langle v_i'^2 \rangle$, to the turbulent kinetic energy are analogous to their Navier–Stokes counterparts. Flux terms within these budgets must be evaluated, as in the derivation of (A 4), based on the conservation laws obeyed by ODT.

Therefore the ODT budget of $\langle v_i'^2 \rangle$ is obtained by first reconsidering (A 1). The usual approach would be to multiply this equation by v_i, average, and then combine the result with $\langle v_i \rangle$ times (A 2) to obtain an evolution equation for $\langle v_i'^2 \rangle$. However, this approach is again inapplicable to the advective terms because of the limited role of the velocity profiles in ODT. Therefore the appropriate starting point is the formal equation

$$\frac{\partial v_i^2}{\partial t} = 2\nu v_i \frac{\partial^2 v_i}{\partial y^2} + M_{ii} + K_{ii}, \tag{A 6}$$

where M_{ii} and K_{ii} represent the effects of the triplet-map and pressure-scrambling operations, respectively, on v_i^2 at given y. For the illustrative case below (A 1), $M_{ii}(y,t) = (\tilde{v}_i^2 - \hat{v}_i^2)\delta(t - t_0)$, where $\hat{v}_i$ and $\tilde{v}_i$ are evaluated before and after the triplet map, and the evaluation of K_{ii} is analogous.

K_{ii}, like K_i, is expressed as a sum of scrambling and transport contributions, $K_{ii} = S_{ii} + T_{ii}$. For a given eddy, transport by definition conserves v_i^2 globally, so $\int T_{ii}\,\mathrm{d}y = 0$. Unlike K_i, K_{ii} is not globally conserved, so $\int K_{ii}\,\mathrm{d}y$ is non-zero in general. S_{ii} is not uniquely defined, though its $\mathrm{d}y$-integral for a given eddy is unique. We choose to define S_{ii} within an eddy as its eddy average, $S_{ii} = (1/l)\int K_{ii}\,\mathrm{d}y$. Though arbitrary, this choice does not have a significant impact on computed results because it only affects the spatial distribution of scrambling within an eddy subject to the integral constraint.

It was noted that T_i should not be interpreted as a pressure-transport effect although it is based on the model subprocess that nominally represents pressure-fluctuation effects. Likewise, T_{ii} is not specifically a pressure-transport effect, although the conventional $\langle v_i'^2 \rangle$ budget, unlike the $\langle v_i \rangle$ budget, has a pressure-transport as well as a turbulent transport term. The sum of M_{ii} and T_{ii} contributions can be interpreted as the ODT analogue of the sum of Navier–Stokes pressure-transport and turbulent transport terms, but the M_{ii} and T_{ii} contributions cannot be decomposed consistently into the individual Navier–Stokes terms. Therefore the advective transport term of the plotted $\langle v_i'^2 \rangle$ and q^2 budgets combines these two terms.

Averaging (A 6) yields the ODT evolution equation for $\langle v_i^2 \rangle$,

$$\frac{\partial}{\partial t}\langle v_i^2 \rangle = \nu \frac{\partial^2}{\partial y^2}\langle v_i^2 \rangle - 2\nu \left\langle \left(\frac{\partial v_i}{\partial y} \right)^2 \right\rangle + \langle M_{ii} \rangle + \langle T_{ii} \rangle + \langle S_{ii} \rangle, \tag{A 7}$$

https://doi.org/10.1017/S0022112001005778 Published online by Cambridge University Press

where the viscous contribution has been rearranged in the usual manner. To obtain the evolution equation for $\langle v_i'^2\rangle$, we subtract $(\partial/\partial t)\langle v_i\rangle^2 = 2\langle v_i\rangle(\partial/\partial t)\langle v_i\rangle$ from (A 7). The subtracted term is evaluated by multiplying (A 2) by $2\langle v_i\rangle$. Performing the subtraction and rearranging the viscous terms in the usual manner gives

$$\frac{\partial}{\partial t}\langle v_i'^2\rangle = \nu\frac{\partial^2}{\partial y^2}\langle v_i'^2\rangle - 2\nu\left\langle\left(\frac{\partial v_i'}{\partial y}\right)^2\right\rangle + \langle M_{ii}+T_{ii}+S_{ii}\rangle - 2\langle M_i+T_i\rangle\langle v_i\rangle. \qquad (A\,8)$$

Adopting the I_i notation introduced in (A 4) and introducing the notation $I_{ii}(y) \equiv \int_y^\infty \mathrm{d}y\,(\langle M_{ii}\rangle + \langle T_{ii}\rangle)$, addition and subtraction of $-2I_i(\partial/\partial y)\langle v_i\rangle$ on the right-hand side of (A 8) gives

$$\frac{\partial}{\partial t}\langle v_i'^2\rangle = \nu\frac{\partial^2}{\partial y^2}\langle v_i'^2\rangle - 2\nu\left\langle\left(\frac{\partial v_i'}{\partial y}\right)^2\right\rangle - 2I_i\frac{\partial}{\partial y}\langle v_i\rangle - \frac{\partial}{\partial y}(I_{ii} - 2\langle v_i\rangle I_i) + \langle S_{ii}\rangle \qquad (A\,9)$$

after some rearrangement. This is not the most useful representation for data reduction. The terms in (A 9) have been organized so that their counterparts in conventional Navier–Stokes budgets (as formulated by Moser *et al.* 1998) can be readily identified.

The first term on the right-hand side of (A 9) is the viscous diffusion term, identical in form to the corresponding term of the conventional $\langle v_i'^2\rangle$ budget. The second term is the ODT analogue of the conventional dissipation term $-2\nu\langle(\partial v_i'/\partial x_j)(\partial v_i'/\partial x_j)\rangle$, which is summed over j but not over i. In ODT, property variations are represented only on the y-coordinate, so the ODT dissipation term corresponds to the $j = 2$ term of this sum. This does not imply that ODT necessarily underestimates the viscous dissipation. The conservation laws obeyed by ODT assure that it will exhibit a balance between total (y-integrated) production and total dissipation plus storage (time derivative), and the model can in principle reproduce all these quantities accurately. Because the model is confined to one spatial dimension, velocity derivatives will be larger in magnitude to achieve a given dissipation level than they are in three-dimensional flow. This is another illustration that ODT may provide a reasonable representation of flow energetics although its representation of flow kinematics differs from three-dimensional turbulence.

As noted earlier, I_i is the ODT analogue of the Reynolds-stress component $\langle v_i'v_2'\rangle$. Accordingly, the third term on the right-hand side of (A 9) corresponds precisely to the conventional production term. For $i = 2$, this implies two non-equivalent ODT representations of the quantity conventionally denoted $\langle v_2'^2\rangle$: one is the ODT v_2-component variance (left-hand side), and the other is I_2.

The next term is a transport term because its form precludes a net gain or loss of total $\langle v_i'^2\rangle$. It subsumes the ODT advective processes (triplet map and kernel implementation), and in this regard is analogous to the sum of conventional turbulent transport and pressure transport, here denoted 'advective transport'. There does not appear to be a physically valid decomposition of the ODT term into the two conventional transport terms. Therefore the sum of conventional terms is compared to the ODT advective transport in plotted budgets.

The quantity S_{ii} has been defined so that its properties are analogous to the conventional pressure–strain term. Though there is some arbitrariness in the definition, it was noted that an integral constraint limits its quantitative impact. $\langle S_{ii}\rangle$ measures pressure scrambling by the mechanism introduced in § 2.2. The transport induced by this mechanism is subsumed in the transport term of (A 9). S_{ii} has been defined so that its sum over components i is zero at all y. Thus, there is no scrambling contribution

https://doi.org/10.1017/S0022112001005778 Published online by Cambridge University Press

to the ODT budget of q^2 (the sum of component variances), just as there is no pressure–strain term in the conventional q^2 budget.

REFERENCES

Aurell, E., Dormy, E. & Frick, P. 1997 Binary-tree models of high-Reynolds-number turbulence. *Phys. Rev.* E **56**, 1692–1698.

Benzi, R., Biferale, L., Tripiccione, R. & Trovatore, E. 1997 (1+1)-dimensional turbulence. *Phys. Fluids* **9**, 2355–2363.

Callen, H. B. 1960 *Thermodynamics*. Wiley.

Chekhlov, A. & Yakhot, V. 1995 Kolmogorov turbulence in a random-force-driven Burgers equation. *Phys. Rev.* E **51**, R2739–R2742.

Constantin, P., Lax, P. D. & Majda, A. 1985 A simple one-dimensional model for the three-dimensional vorticity equation. *Commun. Pure Appl. Maths* **38**, 715–724.

De Gregorio, S. 1990 On a one-dimensional model for the three-dimensional vorticity equation. *J. Statist. Phys.* **59**, 1251–1263.

Dreeben, T. D. & Pope, S. B. 1998 Probability density function/Monte Carlo simulation of near-wall turbulent flows. *J. Fluid Mech.* **357**, 141–166.

Juneja, A., Lathrop, D. P., Sreenivasan, K. R. & Stolovitzky, G. 1994 Synthetic turbulence. *Phys. Rev.* E **49**, 5179–5194.

Kerstein, A. R. 1991 Linear-eddy modelling of turbulent transport. Part 6. Microstructure of diffusive scalar mixing fields. *J. Fluid Mech.* **231**, 361–394.

Kerstein, A. R. 1999*a* One-dimensional turbulence: Model formulation and application to homogeneous turbulence, shear flows, and buoyant stratified flows. *J. Fluid Mech.* **392**, 277–334.

Kerstein, A. R. 1999*b* One-dimensional turbulence – Part 2. Staircases in double-diffusive convection. *Dyn. Atmos. Oceans* **30**, 25–46.

Kerstein, A. R. & Dreeben, T. D. 2000 Prediction of turbulent free shear flow statistics using a simple stochastic model. *Phys. Fluids* **12**, 418–424.

Kerstein, A. R., Schmidt, R. C., Wunsch, S., Ashurst, W. T., Nilsen, V. & Dreeben, T. D. 2001 High-resolution modelling of multiscale transient phenomena in turbulent boundary layers. *Sandia National Laboratories Rep.* SAND2001-8108.

Kim, S. K. & Chung, M. K. 1995 Roles of pressure transport and intermittency for computation of turbulent free shear flows. *Intl J. Heat Fluid Flow* **16**, 194–201.

Kraichnan, R. H. 1962 Turbulent thermal convection at arbitrary Prandtl number. *J. Fluid Mech.* **5**, 1374–1389.

Lorenz, E. N. 1955 Available potential energy and the maintenance of the general circulation. *Tellus* **7**, 157–167.

Moser, R. D., Rogers, M. M. & Ewing, D. W. 1998 Self-similarity of time-evolving plane wakes. *J. Fluid Mech.* **367**, 255–289.

Pope, S. B. 2000 *Turbulent Flows*. Cambridge University Press.

Rogers, M. M. & Moser, R. D. 1994 Direct simulation of a self-similar turbulent mixing layer. *Phys. Fluids* **6**, 903–923.

Stull, R. B. 1988 *An Introduction to Boundary Layer Meteorology*. Kluwer.

Van Slooten, P. R., Jayesh & Pope, S. B. 1998 Advances in PDF modelling for inhomogeneous turbulent flows. *Phys. Fluids* **10**, 246–265.

Vicsek, T. & Barabási, A.-L. 1991 Multi-affine model for the velocity distribution in fully turbulent flows. *J. Phys.* A: *Math. Gen.* **24**, L845–L851.

Wunsch, S. & Kerstein, A. R. 2001 A model for layer formation in stably stratified turbulence. *Phys. Fluids* **13**, 702–712.

https://doi.org/10.1017/S0022112001005778 Published online by Cambridge University Press